Fluid Dynamic Characterization of Operating Conditions for Continuous Flow Blood Pumps

ZHONGJUN J. WU,* JAMES F. ANTAKI,* GREG W. BURGREEN,* KENNETH C. BUTLER,† DOUGLAS C. THOMAS,† AND BARTLEY P. GRIFFITH,*

As continuous flow pumps become more prominent as long-term ventricular assist devices, the wide range of conditions under which they must be operated has become evident. Designed to operate at a single, best-efficiency, operating point, continuous flow pumps are required to perform at off-design conditions quite frequently. The present study investigated the internal fluid dynamics within two representative rotary fluid pumps to characterize the quality of the flow field over a full range of operating conditions. A Nimbus/UoP axial flow blood pump and a small centrifugal pump were used as the study models. Full field visualization of flow features in the two pumps was conducted using a laser based fluorescent particle imaging technique. Experiments were performed under steady flow conditions. Flow patterns at inlet and outlet sections were visualized over a series of operating points. Flow features specific to each pump design were observed to exist under all operating conditions. At off-design conditions, an annular region of reverse flow was commonly observed within the inlet of the axial pump, while a small annulus of backflow in the inlet duct and a strong disturbed flow at the outlet tongue were observed for the centrifugal pump. These observations were correlated to a critical nondimensional flow coefficient. The creation of a "map" of flow behavior provides an additional, important criterion for determining favorable operating speed for rotary blood pumps. Many unfavorable flow features may be avoided by maintaining the flow coefficient above a characteristic critical coefficient for a particular pump, whereas the intrinsic deleterious flow features can only be minimized by design improvement. Broadening the operating range by raising the band between the critical flow coefficient and the designed flow coefficient, is also a worthy goal for design improvement. *ASAIO Journal* 1999; 45:442–449.

Many research groups have been working on continuous flow blood pumps as long-term ventricular assist devices (VADs) for patients with heart failure.[1–4] Continuous flow pumps have several advantages over traditional pulsatile VADs. They can be made compact in size and can be inexpensively produced. Because of the unique properties of blood as the operating fluid, it is essential to optimize fluid dynamic performance to reduce high shear stress, local acceleration, cellular residence time in contact with the material surface, and recirculation within the devices. Although these fluid dynamic behaviors may be tolerable for industrial applications, they promote adverse effects upon blood in clinical applications, potentially leading to dam-

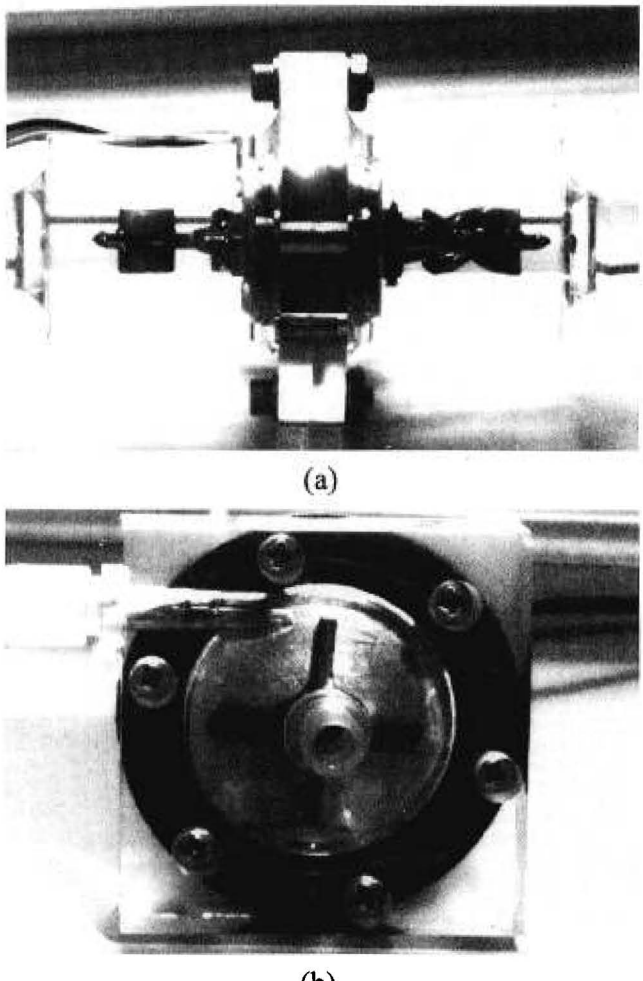

Figure 1. Photographs of (a) the Nimbus/University of Pittsburgh axial flow blood pump and (b) the centrifugal pump used in the study.

From the McGowan Center for Artificial Organ Development, University of Pittsburgh Medical Center, Pittsburgh, Pennsylvania; and †Nimbus, Inc., Rancho Cordova, California.

Submitted for consideration June 1998; accepted for publication in revised form November 1998.

Reprint requests: Zhongjun (Jon) Wu, PhD, 432 McGowan Center for Artificial Organ Development, University of Pittsburgh Medical Center, 300 Technology Drive, Pittsburgh, PA 15219.

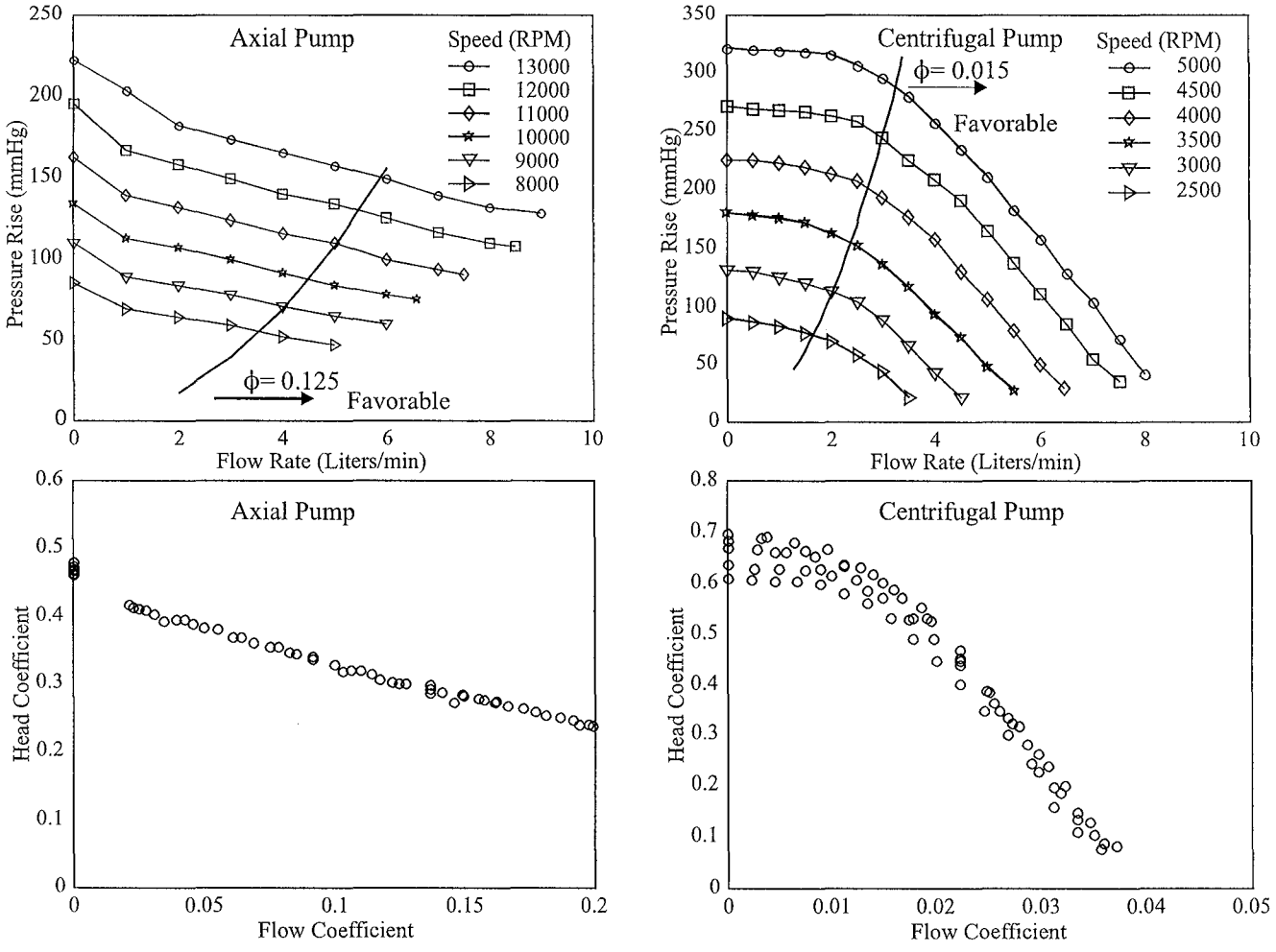

Figure 2. Hydrodynamic characteristics of the two continuous flow pumps. Upper panels indicate the regimes of favorable and unfavorable fluid dynamics. Lower panels provide nondimensional representation of these data.

age and deposition of blood elements in the flow passage. The complex interaction of blood, material, and flow precludes a definitive determination of the probability of thrombosis; however, there is convincing evidence that certain flow dynamics are more favorable than others. Flow visualization has been used extensively as a diagnostic tool to serve this purpose. Several studies have been performed on continuous flow blood pumps to identify unfavorable flow features within the pumps for design improvement.[1,5,6] Traditionally, fluid pumps are designed to operate at a single best efficiency point based on simplified engineering analyses and empiric data. A blood pump used as a long-term VAD is not only required to attain high efficiency at the designed operating point, but it must quite frequently operate over a broad range of physiologic conditions. In spite of the vast quantity of literature on commercial flow pumps and their design,[7,8] and recent use of computational fluid dynamic modelling to optimize flow dynamics within rotary blood pumps,[9] it is virtually impossible to design a pump with ideal fluid dynamic characteristics over the typical physiologic range of cardiac output.

The purpose of the present study was: 1) to illustrate the general relationship between off-design operating conditions and features of the flow field for axial and centrifugal rotary fluid pumps; and 2) to derive a fluid dynamics-based criterion for characterizing the favorable operating zone for these two pumps.

Materials and Methods

A prototype axial flow blood pump housed in a transparent fixture was constructed based on the specifications of an implantable ventricular assist system under development by the joint effort between Nimbus, Inc. (Rancho Cordova, CA) and the University of Pittsburgh (UoP).[10] The pump fluid path consists of a single axial rotor wrapped with three blades, an inlet flow straightener with three straight blades, an outlet stator wrapped with three blades, all within a casing duct. The diameter of the casing duct is 12 mm. **Figure 1a** shows the inlet and outlet sections of the axial pump. The hub of the pump rotor is conically shaped at both ends and cylindrical at the middle. The pump rotor is radially and axially supported by two ball-and-cup bearings located at both ends of the rotor hub. The pump rotor is actuated by an integrated motor, and a permanent magnet within the hub cooperates with field coils located outside the flow tube. The pump was designed to operate at rotor speeds from 8000 rpm to 15,000 rpm with the

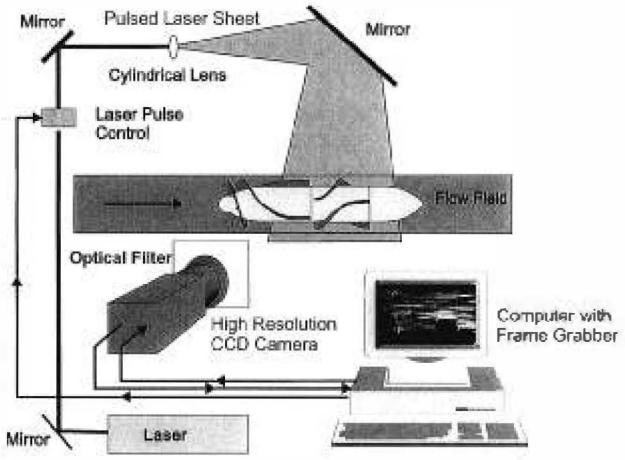

Figure 3. Laser based fluorescent particle imaging system for flow visualization.

best efficiency point at 11,000 rpm at a flow rate of 6.0 L/min against a 100 mm Hg pressure rise.

A commercially available small centrifugal pump (Model 2550–002, Gorman-Rupp Industries, Bellville, OH) was included in the study. The centrifugal pump has a single axial inlet, a primarily cylindrical volute, and a single radial outlet. The pump impeller consists of four straight vanes. The impeller is actuated by a brushless DC motor coupled by a drive shaft through a rubber lip seal. The original front casing of the centrifugal pump was replaced with a transparent replica for flow visualization. **Figure 1b** shows the centrifugal pump.

A transparent blood analog fluid consisting of water/glycerin solution titrated to a viscosity of 3.5 cP and a density of 1.08 g/cm^3 at room temperature (approximately 20°C) was used for all of these studies. The resulting concentration of glycerol was approximately 33% by volume. Although this solution is a Newtonian fluid, it is suitable for these studies because of the high shear rates, in which the non-Newtonian properties of blood such as shear thinning and viscoelasticity are negligible. **Figure 2** shows the hydrodynamic characteristics (H-Q curves) of the two pumps with this working fluid. These characteristics are also plotted in dimensionless forms of the head coefficient ψ and the flow coefficient ϕ[7]:

$$\psi = \frac{gH}{R^2\Omega^2}, \qquad \phi = \frac{Q}{AR\Omega}$$

where H and Q are the head rise and flow rate, respectively; R is the radius of the pump impeller; A is the flow discharge area or the inlet area; Ω is the radian frequency of shaft rotation; and g is the acceleration of gravity. The hydrodynamic characteristic curves of the pumps collapse into nearly one nondimensional curve. The hydrodynamic performance (H-Q curves) of the axial flow pump is identical to that obtained using bovine blood with the same viscosity in our recent study of hemolysis.[11]

A laser based fluorescent particle imaging technique[12] was used to visualize flow patterns within the pumps (see **Figure 3**). Neutrally buoyant fluorescent microspheres, 30 μm in diameter (35–6C, Duke Scientific, Palo Alto, CA), were seeded into the testing fluid as flow markers. A light sheet 1 mm in thickness emanating from an 18 W argon laser (514.5 nm) (Model 171, Spectra Physics, Mountain View, CA) illuminated the flow area of interest within the pump. The circulating fluorescent particles were excited by the laser and emitted light at a longer wavelength (611.0 nm) as the result of the Stokes shift. A high optical contrast was achieved by introducing a high-pass optical filter to attenuate the reflective glare of the excitation light. The illuminated flow area was imaged with a high resolution digital CCD camera (Megplus 1.4, Eastman Kodak Co., San Diego, CA). The images of the flow field were captured through a digital frame grabber board (Oculus-F/64, Coreco, Inc., St-Laurent, Quebec, Canada) at a rate of 10 frames/second. Under each of the selected operating conditions, 1024 × 1024 pixel digital images of the flow field in selected viewing planes were acquired for further analysis.

The flow visualization experiment for the axial pump was performed over a matrix of operating conditions, covering a flow rate range from 1 to 8 L/min in 1 L/min increments at 9, 11, and 13 krpm. The experiment for the centrifugal pump was performed over a flow rate range from 1 to 7 L/min in 1 L/min increments at 4500 rpm. The corresponding flow coefficient ranges to these operating conditions are from 0.02 to 0.20 for the axial pump and from 0.005 to 0.035 for the centrifugal pump, respectively. The above conditions covered the full operating range of the two pumps, as defined by their respective ψ-ϕ characteristics (see **Figure 2**). Flow features were

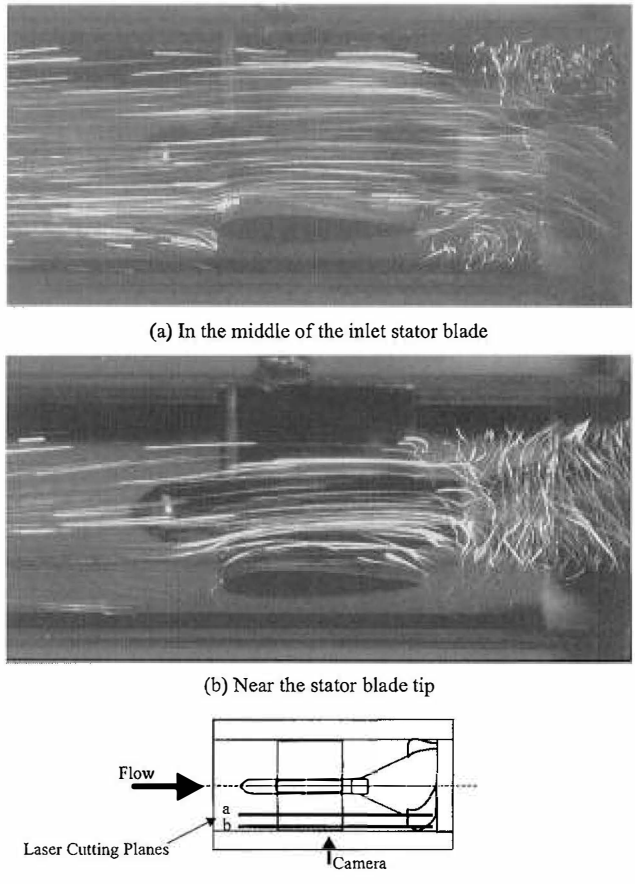

Figure 4. Flow patterns in two viewing planes at the inlet section of the Nimbus/UoP axial flow pump under the nominal operating conditions.

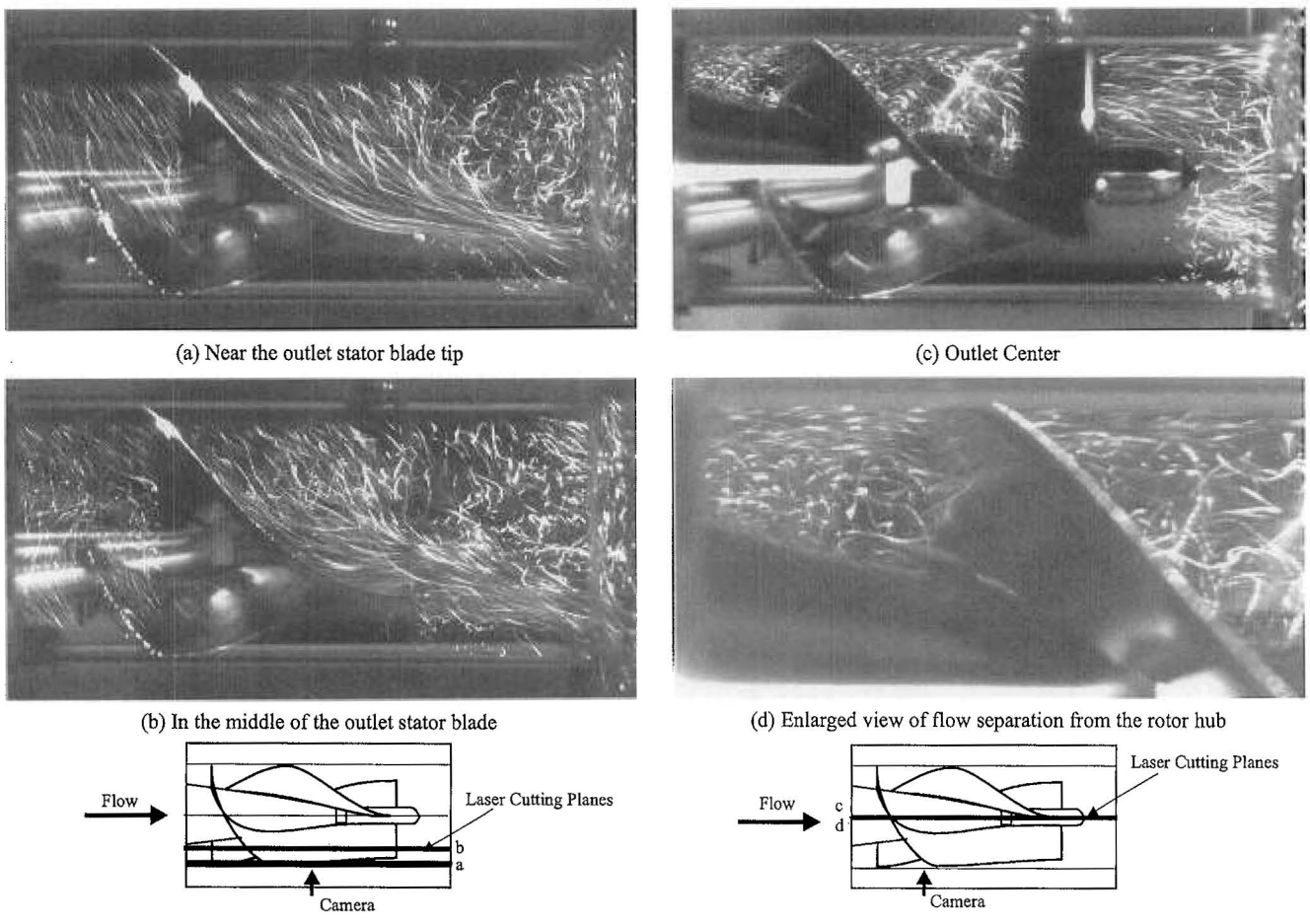

Figure 5. Flow patterns at the outlet section of the Nimbus axial flow pump under nominal operating conditions.

visualized in three viewing planes at the inlet section and three planes at the outlet section for the axial pump; and in two planes at the inlet section, three planes at the outlet section, and one plane in the volute for the centrifugal pump. (The view of the impeller of the axial flow pump was obstructed by the motor field coil.)

Results

Nimbus Axial Pump

The flow within a sector of the inlet flow straightener and aft stator were studied by observing planes from the blade root to tip. **Figure 4** shows the flow patterns in two viewing planes at the inlet section of the axial pump. Under the nominal operating condition, with a flow rate of 6.0 L/min, a pressure rise of 100 mm Hg, and a speed of 11 krpm (flow coefficient: 0.15), the flow within the inlet duct was mostly attached and well behaved. The particle path lines were straight and parallel, except within a small annular region of backflow observed at the rotor blade tip and near the inlet housing wall, and a small recirculation cell observed behind the rather blunt inlet stator blade. **Figure 5** shows the flow patterns in three viewing planes at the outlet section of the axial pump at the same operating condition. The flow features in the outlet duct were rather complex, demonstrating strong three-dimensional characteristics. At the exit of the pump rotor, a layer of helical flow was observed near the outlet stator blade tip, attached to the stator blade and the outlet duct wall (see **Figure 5a**). Less organized flow was observed beneath the layer of the helical flow when the viewing plane was moved to the mid-height of the outlet stator blade (see **Figure 5b**). When the viewing plane was further moved to the centerline, massive separated flow was observed beneath the helical flow layer (see **Figure 5c**). The flow exiting from the rotor impeller blades was separating from the rotor surface before entering the stator blades, ostensibly caused by the expansion of the flow passage (See **Figure 5d**). As the flow further entered into the stator blade region, the helical flow near the blade tip remained attached to the casing wall and the blade surfaces, while the vortices beneath the helical flow propagated and expanded. At the exit of the outlet stator, the particle path lines on the pressure side of the outlet stator blades were mostly attached. Large recirculation cells were observed on the suction side of the blades. Although the exit flow was observed to be chaotic, the flow quickly passed through the outlet stator region and became more organized further downstream after the vortices dissipated.

When operated at higher flow coefficients (> 0.15), the particle path lines were straight within the inlet duct, indicating well organized flow (see **Figure 6a**). The recirculation cell behind the inlet stator blade diminished. However, the same

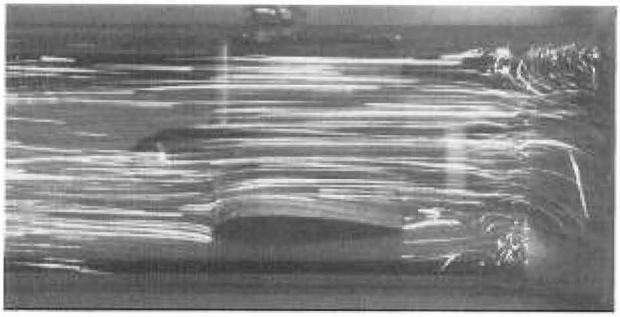

(a) Flow pattern at a high flow coefficient (0.16)

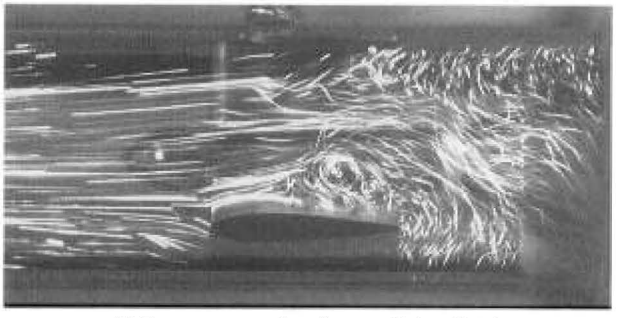

(b) Flow pattern at a low flow coefficient (0.10)

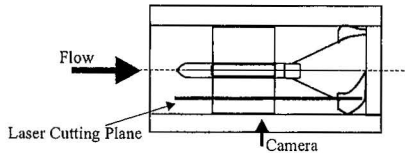

Figure 6. Flow patterns in the inlet duct of the Nimbus axial flow pump at two off-design conditions.

intrinsic flow features were observed in the outlet region as observed under the nominal operating conditions. The incident angle of helical flow to the outlet stator blades increased slightly. A critical flow coefficient, equal to 0.125, was identified, below which a large annular region of backflow was formed in the inlet duct near the casing wall (see **Figure 6b**). After travelling approximately one diameter upstream, the fluid of the backflow region was entrained back into the main inlet flow. The extent and strength of the backflow region increased with decreasing flow coefficient. At the outlet region, the same intrinsic flow features as under all operating conditions studied were observed.

Centrifugal Pump

Figure 7 shows the flow patterns in two viewing planes at the inlet section of the centrifugal pump under the nominal operating conditions (best efficiency point, flow coefficient: 0.025). The inlet flow was characterized by slightly disturbed path lines, originating upstream of the throat and propagating through the distal portion of the tongue. **Figure 8** shows the flow patterns in four viewing planes at the outlet section and within the volute under the same operating conditions. The exit flow in the outlet duct was well attached. A small separation cell was observed near the outer wall of the outlet duct near the front casing wall and back casing wall (see **Figure 8, b and c**). Inside the volute, the majority of particle path lines appeared to spiral radially outward as a result of the discharge through the outflow passage. However, the velocity field beneath the impeller was observed to follow an inwardly spiraling trajectory, indicating radial recirculation and tip leakage beneath the impeller blades (see **Figure 8d**).

Figures 9 and 10 show the flow patterns at the inlet and outlet sections, respectively, of the centrifugal pump at two off-design conditions. As operating conditions departed from the best efficiency point, the overall characteristics of the flow remained similar to those at the best efficiency point. In general, when the centrifugal pump was operated at higher flow coefficients, the flow in the inlet and outlet ducts remained mostly attached (**Figures 9a and 10a**). The particle path lines spiralled more outward in the volute. Separated flow patterns were observed near the outlet tongue where the outward spiral flow was deflected back into the volute owing to a large incident angle. The circular and inward flow features beneath the impeller were still observed to exist. Overall efficiency of the pump decreased with increasing flow coefficient. When operated below a critical flow coefficient (0.0125), the flow patterns within the centrifugal pump became very disturbed. Large separated flow and recirculation cells were observed near the outer wall of the outlet duct. The flow patterns in the volute evidenced circular particle path lines with decreasing flow coefficient (see **Figure 10b**). The degree of change of the flow field in the inlet duct with decreasing flow coefficient was not as severe as in the outflow duct (see **Figure 9a**). Only when the flow coefficient became very low (below 0.005), did the

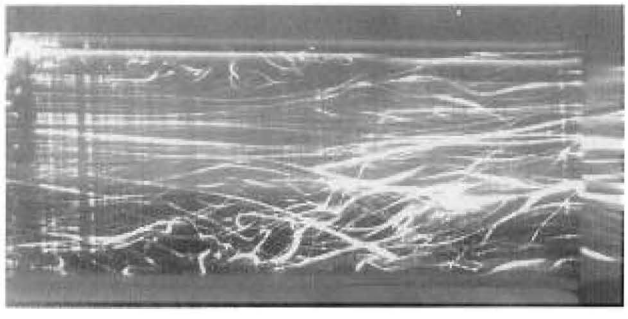

(a) Inlet center cut

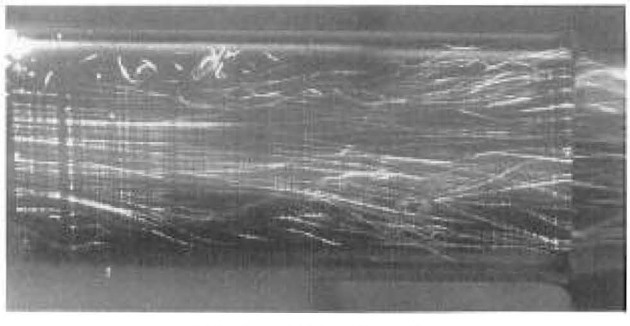

(b) In the middle of the radius

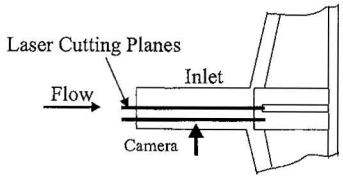

Figure 7. Flow patterns in the inlet duct of the centrifugal pump at the best efficiency point.

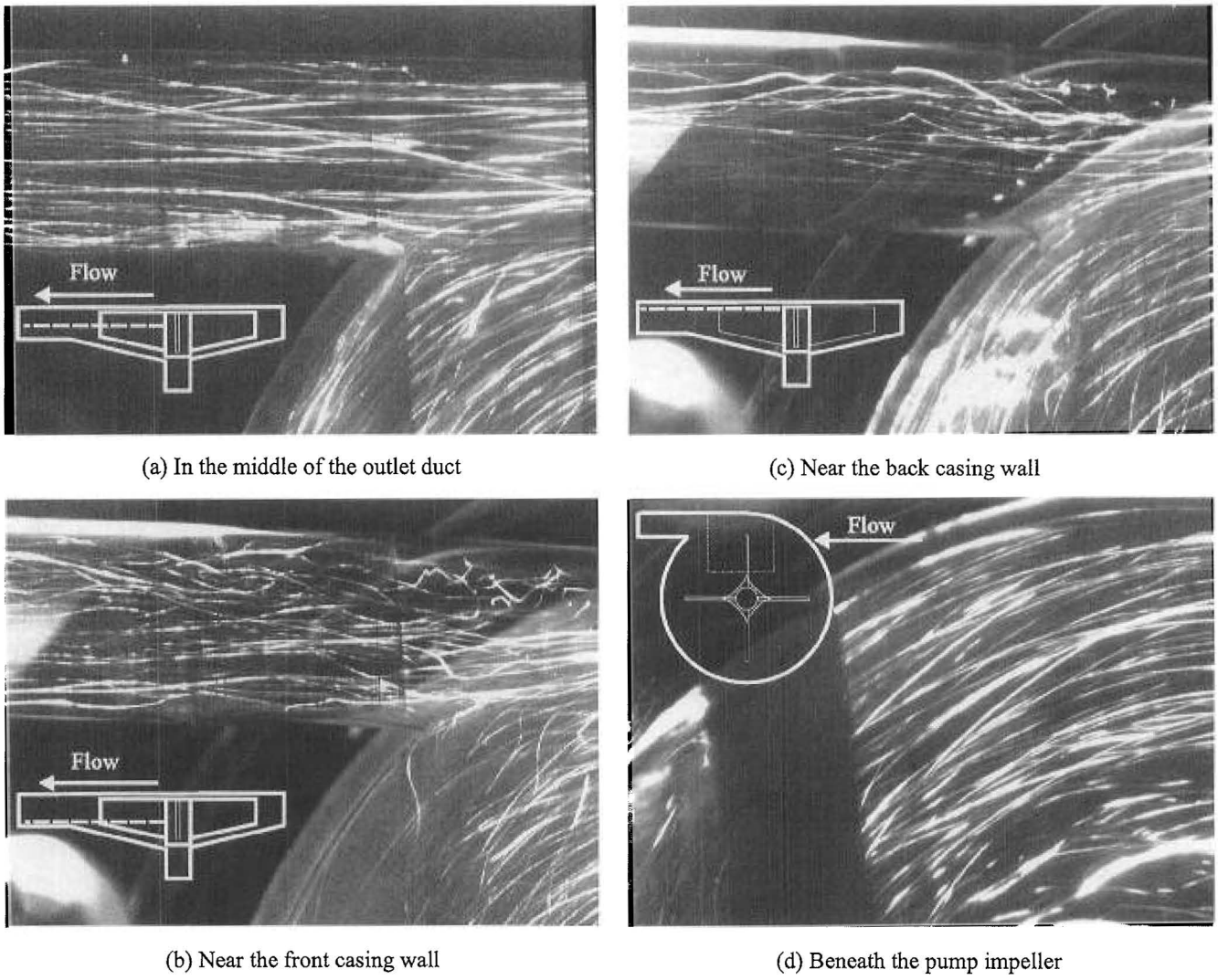

(a) In the middle of the outlet duct

(c) Near the back casing wall

(b) Near the front casing wall

(d) Beneath the pump impeller

Figure 8. Flow patterns in the outlet duct and pump chamber of the centrifugal pump at the best efficiency point.

flow within the diffusing portion of the inflow housing demonstrate slight boundary layer separation, resulting in a toroidal recirculation cell.

Discussion

Although disturbed flow features were observed at the inlet and outlet tracts of the Nimbus/UoP axial flow pump under the nominal operating conditions, the *in vivo* experience with this device has shown an acceptably small degree of red blood cell damage.[4,10] This may be attributed to the rapid passage of cells through the pump, and relatively short residence time, despite local recirculating flow. However, if operated below the critical flow coefficient, the inlet backflow may dramatically increase the exposure time of blood elements to high shear stress. The preliminary results of *in vitro* hemolysis evaluation has shown that the damage level of red blood cells was significantly higher at a low flow coefficient (approximately 0.09) than that at the designed operating point.[11] This is consistent with the observations of other investigators.[13] It is therefore necessary to consider these fluid dynamic characteristics while controlling and operating the pump *in vivo*.

It has been suggested that the annular region of backflow in the inlet duct is caused by the rotor blade tip leakage jet flow.[7] When the pressure difference driving the leakage flow becomes sufficiently large, the impeller tip leakage jet penetrates upstream of the inlet plane of the impeller and forms the annular region of backflow. This flow phenomenon was also reported to exist in several other axial and centrifugal pump designs.[5,7] The observed flow features within the axial flow pump, specifically the backflow in the inlet duct and the flow separation at the rotor exit, were consistent with those predicted from our CFD modeling. Detailed comparison of experimental and CFD results on this axial flow blood pump can be found elsewhere.[9,14] It is anticipated that CFD based design and analysis may prove to be an effective means of mitigating many deleterious flow features found in miniature axial flow blood pumps.

The inward spiralling flow feature found beneath the impeller of the centrifugal pump is an inevitable flow phenomenon, especially for unshrouded impellers. The radial adverse pressure gradient is responsible for driving the fluid near the stationary wall towards the impeller hub. Several earlier studies of

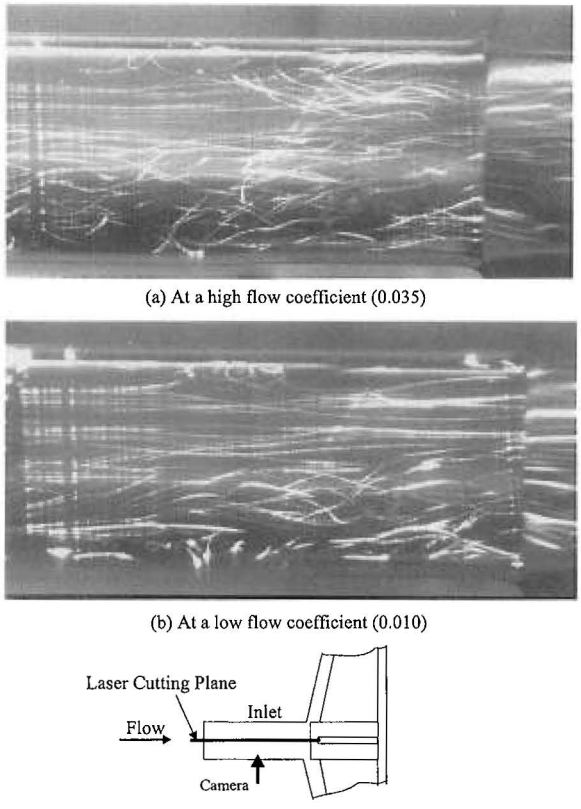

(a) At a high flow coefficient (0.035)

(b) At a low flow coefficient (0.010)

Figure 9. Flow patterns at the inlet of the centrifugal pump at two off-design conditions.

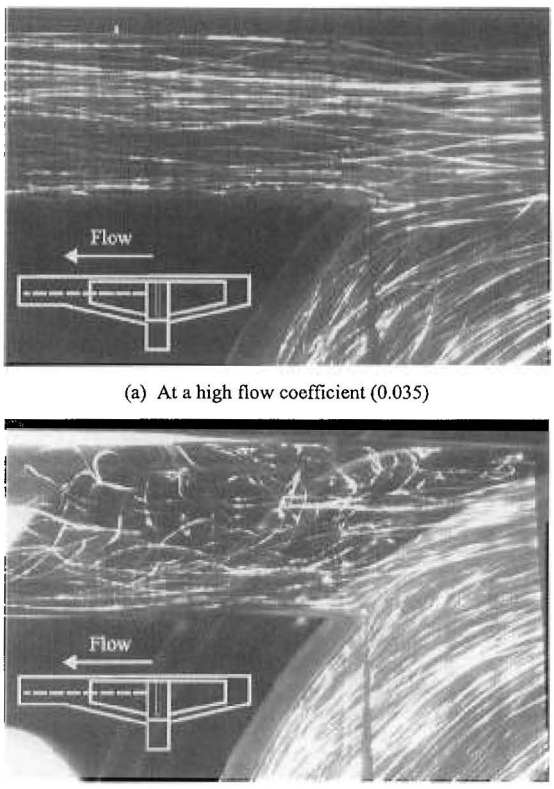

(a) At a high flow coefficient (0.035)

(b) At a low flow coefficient (0.010)

Figure 10. Flow patterns at the outlet section of the centrifugal pump at two off-design conditions.

centrifugal pumps corroborate the existence of this flow aberration.[5,15] The disturbed and separated flows occurring in the outlet volute are also common flow features of centrifugal pumps at off-design conditions.[7]

Conclusion

Two primary types of aberrant flow features were observed within the two continuous flow pumps. The first type of flow structure is intrinsically related to the design geometry of the pump, and includes 1) complex three dimensional path lines at the outlet section and separated flow near the outlet hub in the axial pump, and 2) inward flow beneath the impeller blades and separated flow near the outlet duct wall in the centrifugal pump. The second set of flow features is caused by the selection of operating conditions. These flow features include 1) the annular backflow in the inlet duct of the axial pump, and 2) the large separation cells in the centrifugal pump.

Based on the results of the present study, design modifications have been made to eliminate the intrinsic separated flow in the outlet region of the Nimbus/UoP axial pump. The modified pump is presently undergoing *in vitro* investigation. The observed flow features in the centrifugal pump provide useful insight for further design improvement. The creation of a "map" of flow behavior wherein a critical flow coefficient is identified provides an important criterion for determining the best operating speed for a given pump design.

Acknowledgment

This work was supported jointly by the McGowan Foundation and the National Institutes of Health grant HV-5815.

References

1. Araki K, Taenaka Y, Masuzawa T, *et al*: A flow visualization study of centrifugal blood pumps developed for long-term usage. *Artif Organs* 17: 307–312, 1993.
2. Butler KC, Maher TR, Borovetz HS, *et al*: Development of an axial flow blood pump VAS. *ASAIO J* 38: 296–300, 1992.
3. DeBakey ME: Development of a ventricular assist device. *Artif Organs* 21: 1149–1153, 1997.
4. Macha M, Litwak P, Yamazaki K, *et al*: Survival for up six moths in calves supported with an implantable axial flow ventricular assist device. *ASAIO J* 43: 311–315, 1997.
5. Wernicke JT, Meier D, Mizuguchi K, *et al*: A fluid dynamic analysis using flow visualization of the Baylor/NASA implantable axial flow blood pump for design improvement. *Artif Organs* 19: 161–177, 1995.
6. Ikeda T, Yamane T, Orita T, Tateishi T: A quantitative visualization study flow in a scaled-up model of a centrifugal blood pump. *Artif Organs* 20: 132–138, 1996.
7. Brennen CE: *Hydrodynamics of Pumps.* Oxford, England, Oxford University Press, 1994.
8. Stepanoff J: *Centrifugal and Axial Flow Pumps: Theory, Design, and Application.* 2nd Edition. Maladar, Florida, Krieger Publishing Company, 1957.
9. Burgreen GW, Antaki JF, Wu ZJ, Blanc PL, Butler KC: A computational and experimental comparison of two outlet stators for the Nimbus LVAD. *ASAIO J* 45:XXX-XXX, 1999 (in press).
10. Butler KC, Thomas D, Antaki JF, *et al*: Development of the Nimbus/Pittsburgh axial flow left ventricular assist system. *Artif Organs* 21: 602–607, 1997.
11. Wu ZJ, Kameneva MV, Repko BM, Butler KC, Antaki JF: Relationship between fluid dynamics and hemolysis of an axial flow blood pump. Presented at the 1998 BMES annual meeting, Cleveland, OH, October 1998.

12. Kerrigan JP, Yamazaki K, Meyer RK, *et al*: High-resolution fluorescent particle tracking flow visualization within an intraventricular axial flow left ventricular assist device. *Artif Organs* 20: 534–539, 1996.
13. Mulder MM, Hansen AC, Mohammad SF, DB Olsen: In vitro investigation of the St. Jude Mechanical isoflow centrifugal pump: flow visualization and hemolysis studies. *Artif Organs* 21: 947–960, 1997.
14. Wu ZJ, Burgreen GW, Thomas DC, Butler KC, Griffith BP, Antaki JF: Visualization of flow features in a miniature axial flow blood pump using laser-based fluorescent particle imaging technique. Proc. of 8th International Symposium on Flow Visualization, Italy, September, 1998.
15. Schima H, Huber L, Melvin D, Trubel W, *et al*: Effect of stationary guiding vanes on improvement of the washout behind the rotor in centrifugal blood pumps. *ASAIO J* 38: 220–224, 1992.